ELSEVIER

Journal of Fluids and Structures 20 (2005) 177–187

JOURNAL OF FLUIDS AND STRUCTURES

www.elsevier.com/locate/jfs

Effect of membrane thickness on the slip and drift velocity in parallel shear flow

C. Pozrikidis*

Department of Mechanical and Aerospace Engineering, University of California, San Diego, La Jolla, CA 92093-0411, USA

Received 28 May 2004; accepted 27 October 2004

Abstract

Shear flow past a planar membrane or screen, idealized as an infinite plate perforated by parallel periodic slots, is discussed with emphasis on the effect of the plate thickness on the slip velocity, defined as the displacement of the linear velocity profile on the side of the plate where a shear flow is imposed, and on the drift velocity prevailing on the other side of the membrane. Numerical results based on boundary-element methods for longitudinal and transverse flow show that, while the plate thickness has only a moderate effect on the slip velocity, it has a profound effect on the drift velocity. The structure of the flow near the membrane pores is illustrated in terms of the wall shear stress distribution, the velocity distribution for longitudinal flow, and the streamline pattern for transverse flow. The latter reveals the possible occurrence of counter-rotating eddies inducing a back flow.

1. Introduction

In recent years, the effective macroscopic boundary conditions prevailing at the surface of a permeable membrane have been discussed by several authors for normal and parallel shear flow. In theoretical models, the membrane is idealized either as an infinite plate perforated by holes or slits, or as a two-dimensional matrix consisting of a doubly periodic array of unconsolidated particles. This idealized viewpoint reduces the membrane to a screen, sieve, planar solid matrix, or a thin slab of a porous medium immersed in a viscous liquid. Flow normal to the membrane is driven by a pressure difference whose relation to the flow rate has been the subject of several studies, as reviewed by Wang (2002). At low Reynolds numbers, the relation is linear, yielding Starling's law of biomechanics. Parallel shear flow on one side of the membrane induces a drift velocity parallel to the membrane on the other side. Analysis shows that, when the thickness of the membrane is zero, the drift velocity is equal to the slip velocity, defined as the displacement of the linear velocity profile far above the membrane (Pozrikidis, 2001a). More generally, the drift velocity differs from the slip velocity by an amount that is roughly proportional to the membrane thickness. In the extreme case of flow over a thick membrane resembling a semi-infinite porous medium, the effective fluid velocity decays exponentially with distance normal to the surface of the porous medium, and the drift velocity is effectively zero [e.g., Larson and Higdon (1986, 1987); Tachie et al. (2004)]. An important goal in the study of shear flow over a membrane is to compute the apparent slip and drift velocities in terms of the membrane solidity and detailed geometry.

*Tel.: +1 858 534 6530; fax: +1 853 534 7078.
E-mail address: cpozrikidis@ucsd.edu (C. Pozrikidis).

0889-9746/$ - see front matter © 2005 Elsevier Ltd. All rights reserved.
doi:10.1016/j.jfluidstructs.2004.10.013

Tio and Sadhal (1994) first acknowledged the occurrence of a slip velocity for shear flow over a porous membrane, which is analogous to the slip velocity for flow over the surface of a porous medium, and performed detailed calculations for a model membrane idealized as a zero-thickness plate perforated by parallel slits. More recently, Pozrikidis (2001a) developed an asymptotic expression for the slip velocity for flow past a zero-thickness plate perforated by circular holes. In the discussion, a distinction was made between the slip and drift velocities for a finite-thickness membrane, and numerical results were presented for idealized membranes consisting of doubly periodic arrays of particles and periodic arrays of cylinders. Wang (2001) discussed flow in a two-dimensional channel divided into two compartments by a slotted plane, where the motion is driven by the parallel translation of the channel walls. In all of these calculations, the flow is either unidirectional or governed by the linear equations of Stokes flow applicable at low Reynolds numbers. To assess the effect of the Reynolds number, Pozrikidis (2004) computed numerical solutions of the Navier–Stokes equation for two-dimensional transverse shear flow over a periodic array of cylinders using a finite-difference method, and demonstrated that fluid inertia promotes the magnitude of the slip and drift velocities.

Our main goal of this work is to illustrate the effect of the membrane thickness on the slip and drift velocities based on the flow configuration considered by Tio and Sadhal (1994), in the limit of Stokes flow. Specifically, the analytical results derived by Tio and Sadhal (1994) for flow past a zero-thickness plate perforated by slots will be extended by numerical methods to plates of finite thickness, and the effect of the membrane thickness will be investigated with emphasis on flow kinematics. The numerical solutions of Pozrikidis (2004) suggest that, in the case of transverse flow, inertial effects become significant when the Reynolds number defined with respect to the microscopic membrane dimension is on the order of 100, which is high in the applications motivating this work.

In Sections 2 and 3, unidirectional flow parallel to the slots and two-dimensional flow transverse to the slots are discussed, subject to a specified shear rate above the plate and vanishing shear rate below the plate. In Section 4, effective boundary conditions applicable for a general shear flow with arbitrary shear rates on either side of the plate are considered. The practical significance of the analysis is then demonstrated with reference to the flow in a divided channel considered by Wang (2001).

2. Longitudinal flow

We begin by considering unidirectional shear flow along the z-axis above an infinite plate of finite thickness perforated by a periodic array of parallel slits, as shown in Fig. 1. In this idealized configuration, the plate consists of an infinite sequence of rectangles of width a and depth b separated by the distance L, where the upper surface of the rectangles is located at $y = 0$. Elementary fluid mechanics shows that the z velocity component, u_z, satisfies Laplace's equation

$$\nabla^2 u_z \equiv \frac{\partial^2 u_z}{\partial x^2} + \frac{\partial^2 u_z}{\partial y^2} = 0, \tag{1}$$

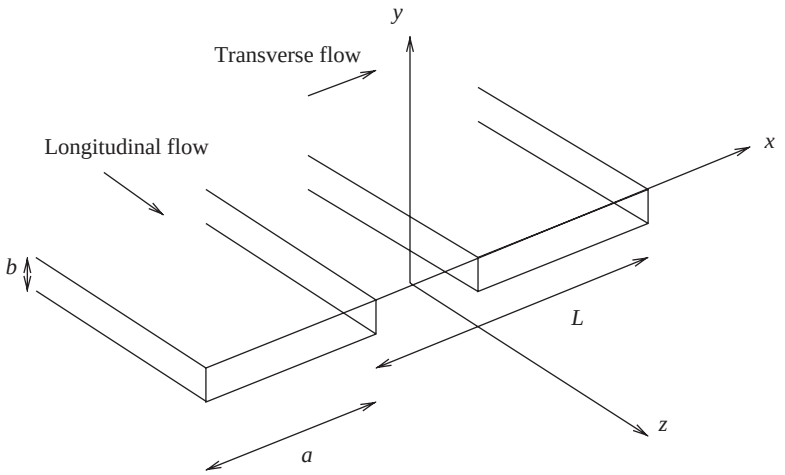

Fig. 1. Schematic illustration of longitudinal or transverse shear flow over a plate perforated by rectangular slits.

subject to the periodicity condition in the x direction, and the far field conditions $\mathrm{d}u_z/\mathrm{d}y \to \gamma$ as $y \to \infty$, and $\mathrm{d}u_z/\mathrm{d}y \to 0$ as $y \to -\infty$, where γ is a specified shear rate. The no-slip boundary condition requires that $u_z = 0$ over the solid surface of the plate.

To develop an integral representation for the flow, we introduce the harmonic potential due to a periodic array of two-dimensional point sinks deployed along the x axis and separated by the distance L, given by

$$G(\mathbf{x},\mathbf{x}_0) = -\frac{1}{4\pi}\log[2\,\cosh(k(y-y_0)) - 2\,\cos(k(x-x_0))] - \frac{1}{2L}(y-y_0), \tag{2}$$

where $k = 2\pi/L$ is the wave number, and $\mathbf{x}_0$ is the position of any one point sink. By construction, this harmonic potential is the periodic Green's function of Laplace's equation, satisfying

$$\nabla^2 G(\mathbf{x},\mathbf{x}_0) + \sum_{n=-\infty}^{\infty} \delta_2(\mathbf{x}-\mathbf{x}_n) = 0, \tag{3}$$

where δ_2 is the two-dimensional delta function in the xy plane, and $\mathbf{x}_n = (x_0 + nL, y_0)$ is the location of the nth point sink. Far above the array, as $(y-y_0) \to \infty$, the periodic Green's function produces a linear field, $G(\mathbf{x},\mathbf{x}_0) \to -(y-y_0)/L + \mathrm{edt}$, where "edt" denotes exponentially decaying terms. Far below the array, as $(y-y_0) \to -\infty$, the periodic Green's function decays at an exponential rate, $G(\mathbf{x},\mathbf{x}_0) \to 0$. A subroutine that evaluates this Green's function is included in the public software libraries FDLIB (Pozrikidis, 2001b) and BEMLIB (Pozrikidis, 2002).

The requisite integral representation arises by applying Green's third identity for the longitudinal velocity field using the periodic Green's function and choosing as control area one period of the flow in the xy plane. The result is

$$u_z(\mathbf{x}_0) = -\frac{1}{\mu}\oint_C G(\mathbf{x},\mathbf{x}_0) f_z(\mathbf{x})\,\mathrm{d}l(\mathbf{x}) + \gamma y_0 + U_S, \tag{4}$$

where C is the contour of one rectangle in the xy plane, f_z is the shear stress exerted on the surface of the rectangles acting in the z direction, and U_S is the slip velocity (Pozrikidis, 2001a). As $y_0 \to \infty$, the first term on the right-hand side decays at an exponential rate, yielding a linear flow with an apparent slip velocity. On the other hand, as $y_0 \to -\infty$, we obtain the drift velocity

$$\begin{aligned} u_z(\mathbf{x}_0) \to U_D &\equiv \frac{1}{\mu}\oint_C \frac{y-y_0}{L} f_z(\mathbf{x})\,\mathrm{d}l(\mathbf{x}) + \gamma y_0 + U_S \\ &= \frac{1}{\mu L}\oint_C y f_z(\mathbf{x})\,\mathrm{d}l(\mathbf{x}) + y_0\left[\gamma - \frac{1}{\mu L}\oint_C f_z(\mathbf{x})\,\mathrm{d}l(\mathbf{x})\right] + U_S. \end{aligned} \tag{5}$$

A force balance over the control volume requires

$$\oint_C f_z(\mathbf{x})\,\mathrm{d}l(\mathbf{x}) = \gamma\mu L \tag{6}$$

Thus, the term enclosed by the square brackets on the right-hand side of (5) is zero, and the slip and drift velocities are related by

$$U_D = \frac{1}{\mu L}\oint_C y f_z(\mathbf{x})\,\mathrm{d}l(\mathbf{x}) + U_S. \tag{7}$$

In the case of flow over a flat plate of zero thickness located at y_p considered by Tio and Sadhal (1994), corresponding to $b = 0$, we use the aforementioned force balance to obtain

$$U_D = \gamma y_p + U_S, \tag{8}$$

which shows that, if the origin of the y-axis is pinned at the plate, as it is under the present convention, the slip and drift velocities are equal. Tio and Sadhal (1994) were able to derive the exact result

$$U_S = -\frac{\gamma L}{2\pi}\log\left[\cos\left(\frac{\pi}{2}\left(1-\frac{a}{L}\right)\right)\right]. \tag{9}$$

As $a/L \to 1$, the slits disappear and the slip velocity tends to zero; on the other hand, as $a/L \to 0$, the slip velocity diverges at a logarithmic rate.

Applying the integral representation (4) at the surface of the plates, and requiring the no-slip boundary condition, $u_z = 0$, we obtain an integral equation of the first kind for the shear stress,

$$\oint_C G(\mathbf{x}, \mathbf{x}_0) f_z(\mathbf{x})\, \mathrm{d}l(\mathbf{x}) - \mu U_S = \mu\gamma y_0, \tag{10}$$

where the point $\mathbf{x}_0$ lies on C. Appending to this equation the integral constraint (6), we obtain a self-contained system of governing equations. This system was solved by a standard boundary-element method, featuring graded element discretization with high concentration near the corners [e.g., Pozrikidis (2002)]. By way of illustrating the numerical accuracy, we note that, for a test case in which the plate consists of periodic repetition of rectangles of width $a/L = 0.5$ and depth $b/L = 0.5$, the numerical method yields the reduced slip velocity $U_S/(\gamma L) = 0.04252$, 0.04200, 0.04179, 0.04171, and 0.04168, respectively, for 32, 64, 128, 256, and 512 boundary elements around the four sides of the rectangular contour. This test suggests that accuracy up to the fourth decimal place can be obtained with a modest number of elements. The boundary-element code is included in the public software libraries FDLIB (Pozrikidis, 2001b) and BEMLIB (Pozrikidis, 2002).

Fig. 2 shows graphs of the slip and drift velocities, both reduced by the Tio and Sadhal (1994) value for a zero-thickness plate given in (9), plotted against the reduced plate thickness, b/L, for plate solidity $a/L = 0.5$ and 0.2. In both cases, the reduced slip velocity shown with the solid line decreases from the value of unity at $b/L = 0$, to an asymptotic value that is approximately equal to 0.75 for $a/L = 0.5$, or 0.6 when $b/L = 0.20$. The asymptotic value at infinity corresponds to infinite shear flow over a surface containing a periodic sequence of rectangular, semi-infinite fins. Correspondingly, the reduced drift velocity shown with the broken line decays from the value of unity at $b/L = 0$, to the asymptotic value of zero as $b/L \to \infty$. Thus, while the plate thickness has only a moderate effect on the slip velocity, it does have a profound effect on the drift velocity.

Fig. 3(a,b) illustrates the spatial structure of the reduced longitudinal velocity, $v \equiv u_z/(\gamma L)$, for $a/L = 0.5$ and 0.2, and a fixed plate thickness, $b/L = 0.25$. Fig. 3(c,d) illustrates the corresponding distribution of the wall shear stress, f_z, plotted with respect to arc length, s, measured around the perimeter of a rectangle in the counterclockwise direction, starting from the southeastern corner. The shear stress exhibits an integrable singularity at the four corners, as predicted by a local analysis of Laplace's equation. The singularity is captured with adequate accuracy in the boundary-element solution thanks to the increased local element concentration. Comparison between the two distributions shown in Fig. 3(c,d) shows that, as the solidity a/L is reduced, the flow is able to penetrate more effectively the lower surface of the plate, and the magnitude of the shear stress over the bottom side tends to become comparable to that on the upper side. Evidence for this behavior is also found by a careful inspection of the velocity field shown in Fig. 3(a, b). Near the middle of the upper surface of the plate, the shear stress is comparable to that of the unperturbed flow for $a/L = 0.5$, and nearly twice as high for $a/L = 0.2$.

3. Transverse flow

Next, we turn our attention to the complementary case of two-dimensional transverse shear flow along the x-axis above the perforated plate, as shown in Fig. 1. At sufficiently small Reynolds numbers, $\mathrm{Re} = \rho\gamma L^2/\mu$, where ρ is the fluid density, the fluid motion is governed by the continuity equation, $\nabla \cdot \mathbf{u} = 0$, and the Stokes equation,

$$-\nabla p + \mu\nabla^2 \mathbf{u} = 0, \tag{11}$$

where $\mathbf{u} = (u_x, u_y)$ is the velocity, p the pressure, and μ the fluid viscosity. The velocity and pressure are periodic in the x direction, and the y velocity component decays to zero far from the plate. The far-field condition requires $\mathrm{d}u_x/\mathrm{d}y \to \gamma$ as $y \to \infty$, and $\mathrm{d}u_x/\mathrm{d}y \to 0$ as $y \to -\infty$, where γ is a specified shear rate. The no-slip boundary condition requires that both velocity components are zero over the solid surface of the plate.

To develop an integral representation for the flow, we introduce the velocity field due to a periodic array of two-dimensional point forces of strength $\mathbf{b}$, deployed along the x-axis and separated by the distance L, given by $u_i(\mathbf{x}) = G_{ij}(\mathbf{x}, \mathbf{x}_0) b_j/(8\pi\mu)$, for $j = x, y$, where the tensor $G_{ij}(\mathbf{x}, \mathbf{x}_0)$ is the velocity Green's function of periodic Stokes flow. Together with the corresponding pressure Green's function, p_i, the velocity Green's function satisfies the singularly-forced Stokes equation

$$-\frac{\partial p_i}{\partial x_j} + \mu\nabla^2 G_{ji} + 8\pi\delta_{ij} \sum_{n=-\infty}^{\infty} \delta_2(\mathbf{x} - \mathbf{x}_n) = 0, \tag{12}$$

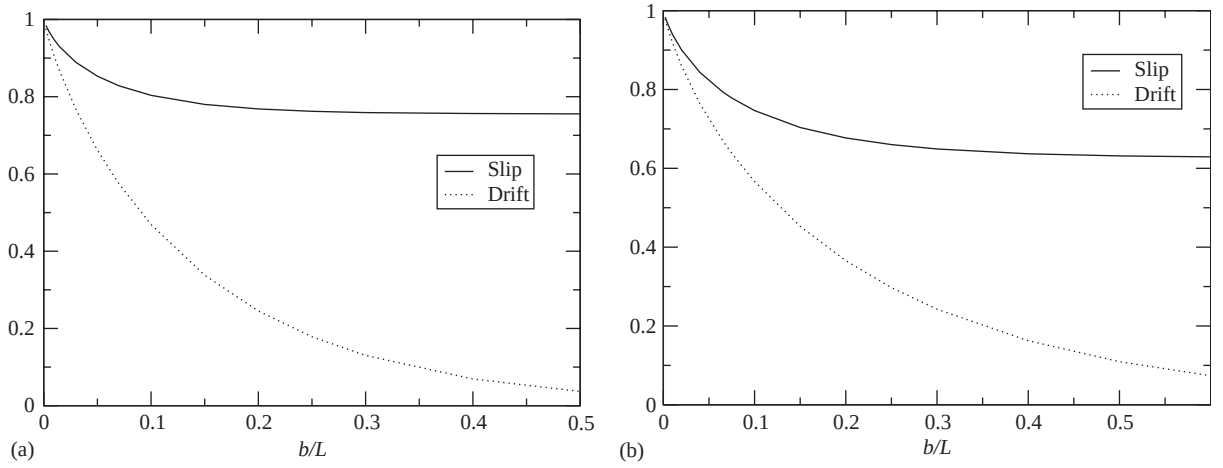

Fig. 2. Effect of plate thickness on the slip and drift velocities, both normalized with respect to Tio and Sadhal (1994) value, for longitudinal flow over a plate with (a) $a/L = 0.5$, and (b) 0.2.

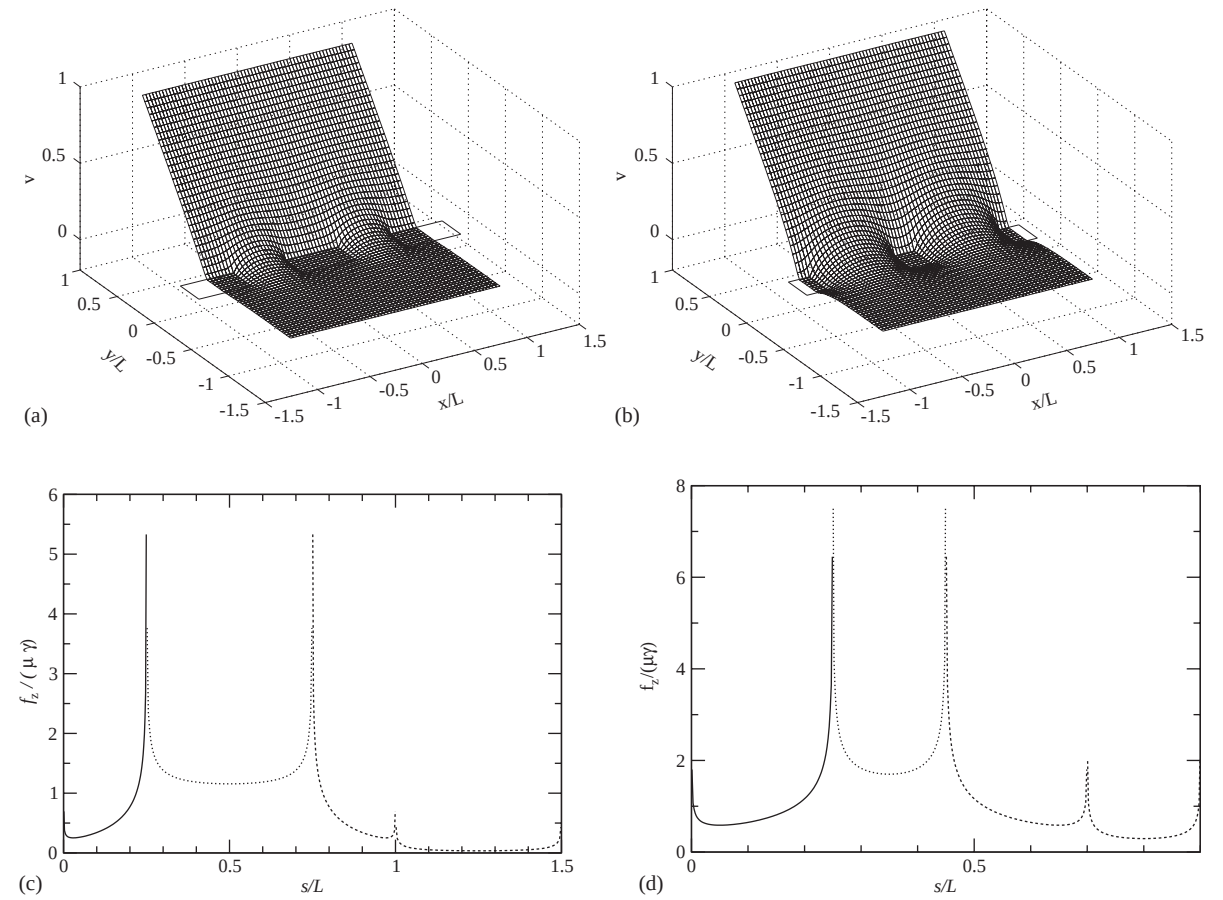

Fig. 3. Velocity field for longitudinal flow over a plate with (a) $a/L = 0.5$, $b/L = 0.25$, and (b) $a/L = 0.2$, $b/L = 0.25$. Frames (c, d) show the corresponding distribution of the wall shear stress plotted with respect to arc length around the rectangles; the solid, dotted, dashed, and dot-dashed lines correspond, respectively, to the right, top, left, and bottom side.

where δ_2 is the two-dimensional delta function in the xy plane, $\mathbf{x}_n = (x_0 + nL, y_0)$ is the location of the nth point force, $\mathbf{x}_0$ is the position of any one point force, and δ_{ij} is Kronecker's delta. The Stokes-flow Green's function can be computed in terms of the corresponding Green's function of Laplace's equation, G, given in Eq. (2), as $G_{ij} = 2\pi Q_{ij}$, where

$$Q_{xx} = G + (y - y_0)\,\frac{\partial G}{\partial y}, \quad Q_{xy} = Q_{yx} = -(y - y_0)\,\frac{\partial G}{\partial x},$$
$$Q_{yy} = G - (y - y_0)\,\frac{\partial G}{\partial y}. \tag{13}$$

Far above the array of point forces, as $(y - y_0) \to \infty$, the periodic Green's function produces a linear field, $G_{xx}(\mathbf{x}, \mathbf{x}_0) \to -2\pi(y - y_0)/L + \text{edt}$, while all other components decay at an exponential rate. Far below the array, as $(y - y_0) \to -\infty$, all Green's function components decay at an exponential rate. A subroutine that evaluates this Green's function is included in the public software libraries FDLIB (Pozrikidis, 2001b) and BEMLIB (Pozrikidis, 2002).

An integral representation for the flow can be derived by applying the reciprocal theorem for Stokes flow for the shear flow of interest and the flow due to periodic array of point forces, choosing as a control area one period of the flow. Using a well-established formalism, we obtain

$$u_j(\mathbf{x}_0) = -\frac{1}{4\pi\mu}\oint_C G_{ij}(\mathbf{x}, \mathbf{x}_0) f_i(\mathbf{x})\, \mathrm{d}l(\mathbf{x}) + \delta_{jx}(\gamma y_0 + U_S), \tag{14}$$

where C is the contour of one rectangle in the xy plane, $\boldsymbol{f}$ is the boundary traction, and U_S is the slip velocity (Pozrikidis, 2001a). As $y_0 \to \infty$, the first term on the right-hand side decays at an exponential rate, yielding a linear flow along the x-axis with an apparent slip velocity. On the other hand, as $y_0 \to -\infty$, we obtain the corresponding drift velocity

$$U_D = \frac{1}{\mu L}\oint_C y f_x(\mathbf{x})\, \mathrm{d}l(\mathbf{x}) + U_S. \tag{15}$$

In the case of flat plates of zero thickness located at $y = y_p$ considered by Tio and Sadhal (1994), $b = 0$, we use the force balance

$$\oint_C f_x(\mathbf{x})\, \mathrm{d}l(\mathbf{x}) = \gamma\mu L, \tag{16}$$

to obtain Eq. (8), which shows that, if the origin of the y-axis is placed on the plate, the slip and drift velocities are equal. Tio and Sadhal (1994) derived the exact result

$$U_S = -\frac{\gamma L}{4\pi}\log\left[\cos\left(\frac{\pi}{2}\left(1 - \frac{a}{L}\right)\right)\right], \tag{17}$$

which differs from the corresponding expression for longitudinal flow, given in Eq. (9), only by a factor of 2. Thus, for a zero-thickness plate, the slip velocity for longitudinal flow is twice that for transverse flow for a given shear rate, γ. Based on this observation, Tio and Sadhal (1994) noted that a shear flow in a certain direction above the plate induces a drift flow in a generally different direction below the plate.

Applying the integral representation (14) at the solid surface of the plate, and requiring the no-slip boundary condition, $u_z = 0$, we obtain an integral equation of the first kind for the boundary traction

$$\oint_C G_{ij}(\mathbf{x}, \mathbf{x}_0) f_i(\mathbf{x})\, \mathrm{d}l(\mathbf{x}) - 4\pi\mu U_S \delta_{jx} = 4\pi\mu\gamma y_0 \delta_{jx}, \tag{18}$$

where the point $\mathbf{x}_0$ lies on C. Appending to this equation the integral constraint (16), we obtain a self-contained system of governing equations. The system was solved by a standard boundary-element method, similar to that discussed in Section 2 for longitudinal flow. By way of demonstrating the accuracy of the numerical method, we note that, for a test case in which the plate consists of periodic repetition of rectangles of width $a/L = 0.5$ and depth $b/L = 0.5$, we obtain the reduced slip velocity $U_S/(\gamma L) = 0.01833$, 0.01810 and 0.01800, respectively, for 64, 128, and 256 boundary elements around the rectangular contour. Thus, accuracy up to the fourth decimal place can be obtained with a modest number of elements. The boundary-element code is included in the public software libraries FDLIB (Pozrikidis, 2001b) and BEMLIB (Pozrikidis, 2002).

Fig. 4 shows graphs of the slip and drift velocities, both reduced by the Tio and Sadhal (1994) value for a zero-thickness plate given in (17), plotted against the reduced plate thickness, b/L, for plate solidity $a/L = 0.5$ and 0.2. In

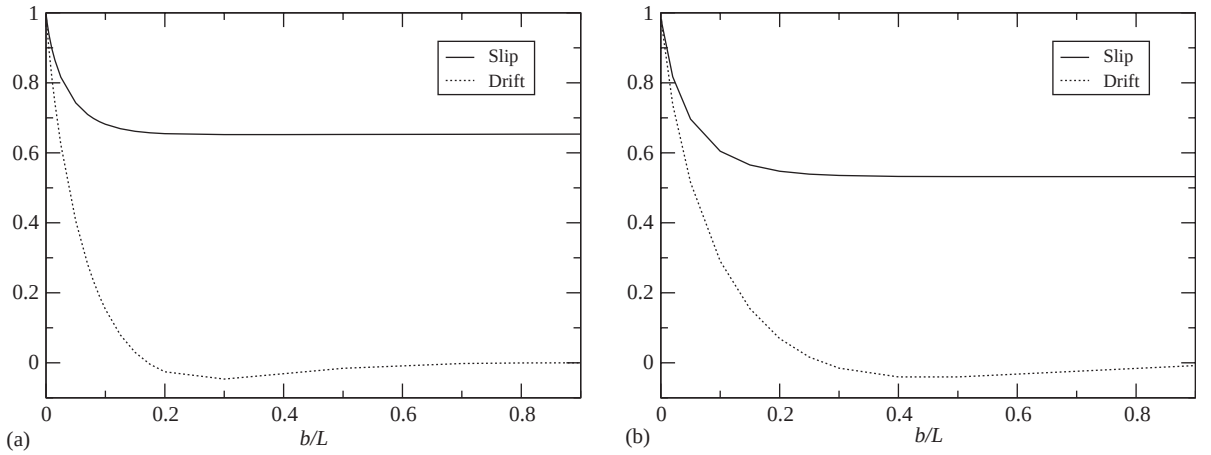

Fig. 4. Effect of plate thickness on the slip and drift velocities, both normalized with respect to Tio and Sadhal (1994) value, for transverse flow over a plate with (a) $a/L = 0.5$, and (b) 0.2.

both cases, the reduced slip velocity shown with the solid line decreases from the value of unity at $b/L = 0$, to an asymptotic value that is approximately equal to 0.65 for $a/L = 0.5$, and 0.52 when $b/a = 0.20$. The asymptotic value at infinity corresponds to infinite shear flow across a modulated surface containing a periodic sequence of semi-infinite rectangular depressions. For $a/L = 0.5$, as the plate thickness b/L increases from the value of zero, the reduced drift velocity shown with the broken line decreases from the value of unity, it becomes negative when $b/L \sim 0.17$, it reaches a minimum, and then it becomes positive again when $b/L \sim 0.90$. For $a/L = 0.2$, the drift velocity first changes sign when $b/L \sim 0.275$. Thus, as in the case of longitudinal flow, whereas the plate thickness has only a moderate effect on the slip velocity, it has a profound effect on the drift velocity. In it worth noting that, in the case of transverse flow over a periodic array of circular cylinders, the slip velocity becomes negative when the cylinder radius is larger than approximately $0.15L$, but this only occurs when the origin of the y axis is set at the cylinder center instead of the uppermost surface (Pozrikidis, 2001a).

The physical reason for the occurrence of a negative drift velocity is the onset of viscous eddies in the gaps between successive rectangles, as illustrated in Fig. 5 for $a/L = 0.5$, and in Fig. 6 for $a/L = 0.2$. The drift velocity is positive for the flows illustrated in Fig. 5(a–c), negative for the flows illustrated in Fig. 5(d,e), and positive again for the flow illustrated in Fig. 5(f). The second change is sign is due to the development of two regions of recirculating fluid, yielding a pair counter-rotating eddies inside the gap. Fig. 4(a) shows that the magnitude of the drift velocity corresponding to Fig. 5(d–f) is small compared to that of the slip velocity, that is, the flow underneath the array is extremely weak. The drift velocity is positive for the flows illustrated in Fig. 6(a,b), and negative for the flow illustrated in Fig. 6(c,d).

Fig. 7 shows the distribution of the wall shear stress, σ_S, for the flows depicted in Fig. 5(e) and 6(c). An integrable singularity is evident in both distributions at the top corners, consistent with a local similarity solution for Stokes flow (e.g., Pozrikidis, 1997). A change in the sign of the shear stress marks a wall stagnation point where a dividing streamline separates regions of counter-flowing fluid. Comparison between the two distributions shows that, as the solidity a/L is reduced, the flow is able to penetrate more effectively the lower side of the plate. Near the middle of the upper surface of the plate, the shear stress is somewhat higher than that of the unperturbed flow for $a/L = 0.5$, and nearly twice as high for $a/L = 0.2$.

4. Discussion

The modular flow configurations considered in Sections 2 and 3 can be readily generalized to shear flow with arbitrary shear rates above and below the plate. To illustrate this extension, we consider unidirectional shear flow along the z-axis parallel to the slots shown in Fig. 1, and assume that, far above and below the array, the velocity profile exhibits the asymptotic distribution

$$u_z^{+\infty} = \gamma_+ y + L(\gamma_+ c_{++} - \gamma_- c_{-+}) + \text{edt},$$
$$u_z^{-\infty} = \gamma_- y + L(\gamma_+ c_{+-} - \gamma_- c_{--}) + \text{edt}, \tag{19}$$

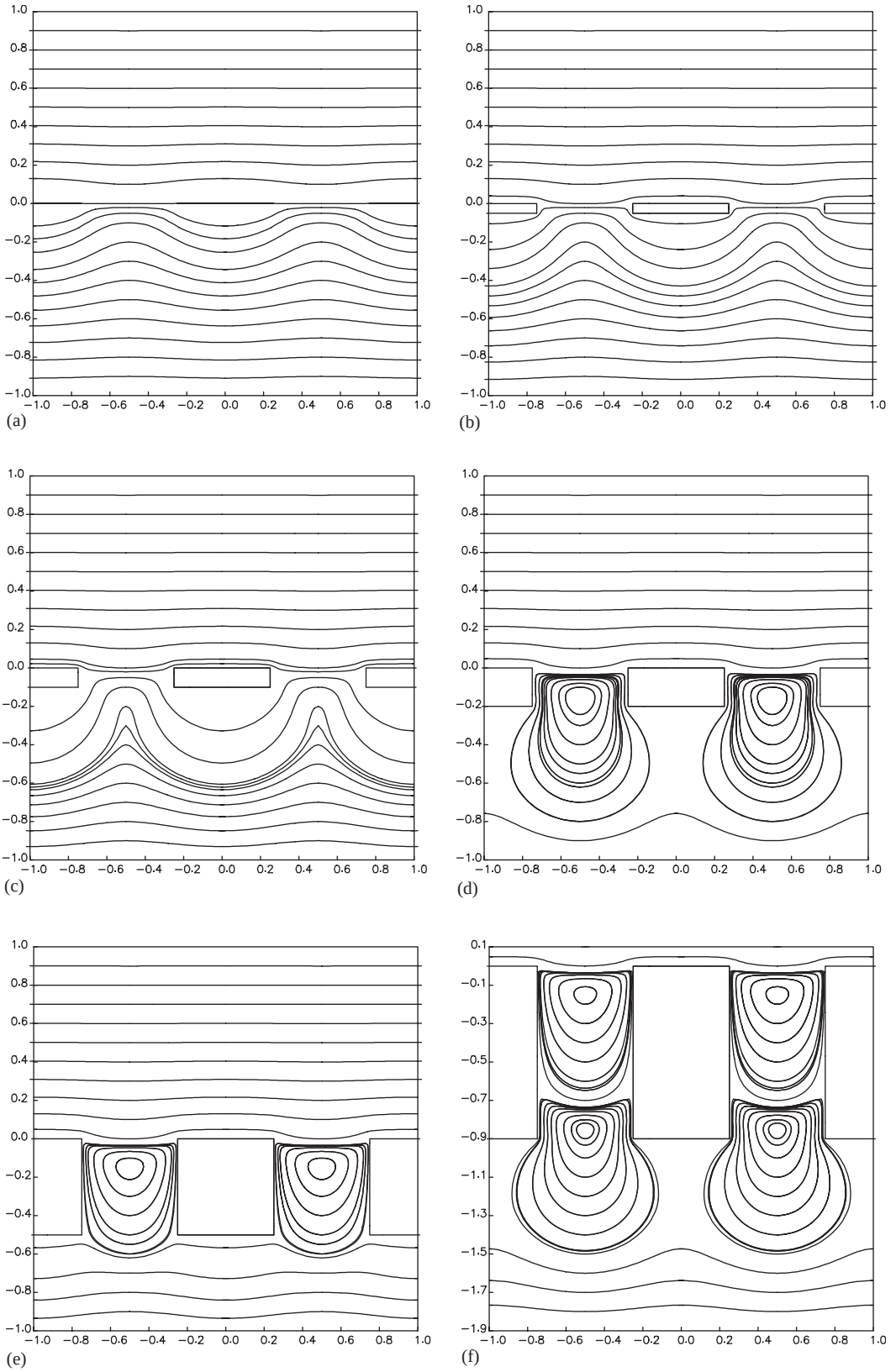

Fig. 5. Streamline pattern of transverse shear flow over a plate of thickness $a/L = 0.5$ and depth (a) $b/L = 0.004$, (b) 0.05, (c) 0.1, (d) 0.2, (e) 0.5, and (f) 0.9.

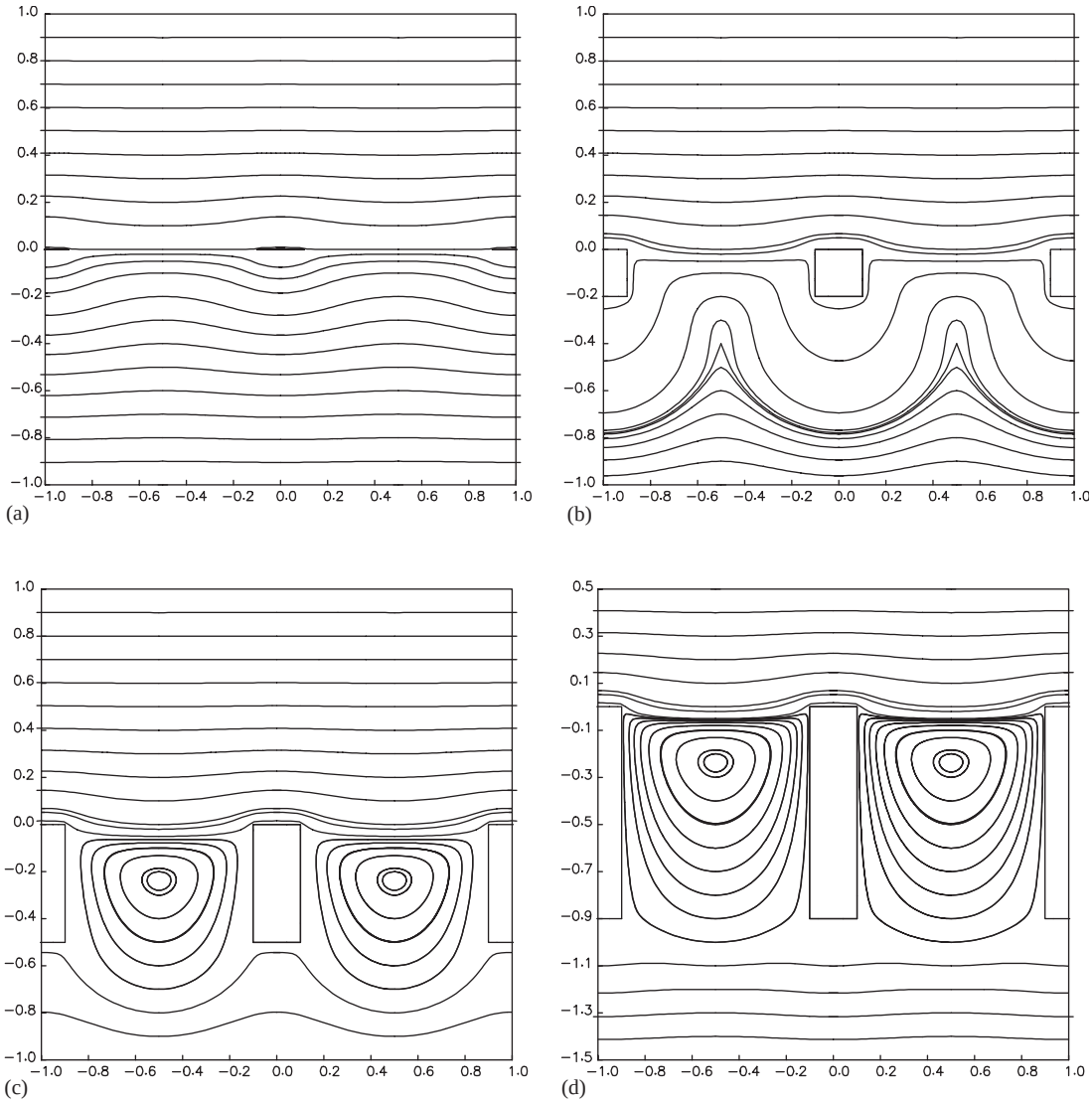

Fig. 6. Streamline pattern of transverse shear flow over a plate of thickness $a/L = 0.2$ and depth (a) $b/L = 0.001$, (b) 0.2, (c) 0.5, and (d) 0.9.

where $\gamma_\pm$ are prescribed constant shear rates, and $c_{\pm\pm}$ are dimensionless coefficients. In Section 2, we considered the case $\gamma_+ = \gamma$ and $\gamma_- = 0$, and computed the slip velocity coefficient c_{++} and drift velocity coefficient c_{+-}. Pretending that the linear velocity profiles expressed by all but the omitted terms on the right-hand sides of (19) can be extended all the way up to the origin of the y-axis, we set $y = 0$ and compute the apparent slip-velocities

$$u_z^{+s} = L(\gamma_+ c_{++} - \gamma_- c_{-+}), \quad u_z^{-s} = L(\gamma_+ c_{+-} - \gamma_- c_{--}), \tag{20}$$

and the apparent discontinuity in the far-field velocity across the array,

$$\Delta u_z \equiv u_z^{+s} - u_z^{-s} = L[\gamma_+(c_{++} - c_{+-}) + \gamma_-(c_{--} - c_{-+})]. \tag{21}$$

For a plate with top-to-bottom symmetry, we put the origin of the y-axis midway between the upper and lower surface, and set $c_{++} = c_{--} \equiv c_S$ and $c_{+-} = c_{-+} \equiv c_D$, to obtain

$$u_z^{+s} = L(\gamma_+ c_S - \gamma_- c_D), \quad u_z^{-s} = L(\gamma_+ c_D - \gamma_- c_S) \tag{22}$$

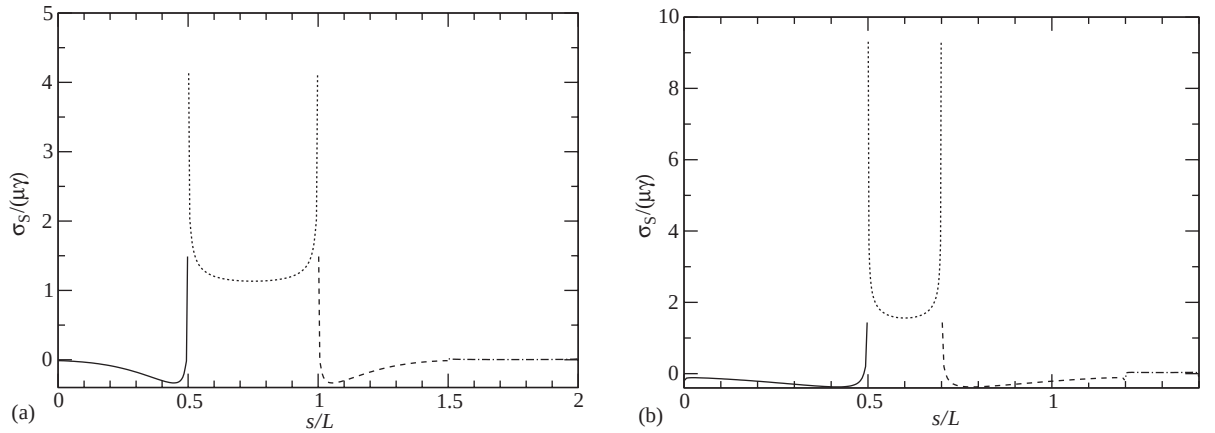

Fig. 7. Distribution of the wall shear stress in transverse flow, plotted with respect to arc length around the rectangle, for (a) $a/L = 0.5$ and $b/L = 0.5$, corresponding to Fig. 5(e), and (b) $a/L = 0.2$ and $b/L = 0.5$, corresponding to Fig. 6(c). The solid, dotted, dashed, and dot-dashed lines correspond, respectively, to the right, top, left, and bottom side.

and

$$\Delta u_z \equiv u_z^{+s} - u_z^{-s} = L(\gamma_+ + \gamma_-)(c_S - c_D), \tag{23}$$

where c_S and c_D are slip and drift velocity coefficients. For a zero-thickness plate considered by Tio and Sadhal (1994),

$$c_S = c_D = -\frac{1}{2\pi}\log\Big[\cos\Big(\frac{\pi}{2}\Big(1 - \frac{a}{L}\Big)\Big)\Big]. \tag{24}$$

Similar equations can be written for the case of two-dimensional shear flow parallel to the x-axis.

To put these results into practical use, we consider a macroscopically unidirectional plane Couette flow in a two-dimensional channel confined between two plane walls located at $y = \pm h$. The channel is divided into two compartments separated by a stationary permeable interface of small thickness, located at $y = y_0$. Elementary derivations show that the macroscopic streamwise velocity profile in the lower and upper compartments have, respectively, the linear forms

$$u^- = U_1 + \gamma_-(y + h), \quad u^+ = U_2 + \gamma_+(y - h), \tag{25}$$

where U_1 and U_2 are the velocities of the lower and upper wall, $h_1 = h + y_0$ and $h_2 = h - y_0$ are the lower and upper compartment heights, and $u^{\pm s}$ are macroscopic slip velocities that depend on the lower and upper shear rates,

$$\gamma_- \equiv \frac{u^{-s} - U_1}{h_1}, \quad \gamma_+ \equiv \frac{U_2 - u^{+s}}{h_2}. \tag{26}$$

Substituting (26) in the generic form of (22) for longitudinal or transverse flow, we find

$$\begin{aligned} u^{+s} &= L\Big(\frac{U_2 - u^{+s}}{h_2}\, c_S - \frac{u^{-s} - U_1}{h_1}\, c_D\Big), \\ u^{-s} &= L\Big(\frac{U_2 - u^{+s}}{h_2}\, c_D - \frac{u^{-s} - U_1}{h_1}\, c_S\Big), \end{aligned} \tag{27}$$

which can be rearranged into the linear system for u^{+s} and u^{-s},

$$\begin{aligned} \Big(1 + \frac{L}{h_2}\, c_S\Big)u^{+s} + \frac{L}{h_1}\, c_D u^{-s} &= \frac{L}{h_2}\, c_S U_2 + \frac{L}{h_1}\, c_D U_1, \\ \frac{L}{h_2}\, c_D u^{+s} + \Big(1 + \frac{L}{h_1}\, c_S\Big)u^{-s} &= \frac{L}{h_2}\, c_D U_2 + \frac{L}{h_1}\, c_S U_1. \end{aligned} \tag{28}$$

Solving this linear system allows us to evaluate the upper and lower slip velocities, $u^{\pm s}$, and thereby generate the velocity profile and compute the shear stress exerted on the channel walls.

One of the coefficients on the left-hand side of the linear system (28) has the general form Lc_S/h_1, and other coefficients are defined by similar expressions. Substituting the Tio and Sadhal (1994) value given in Eq. (24), we find

$$\frac{L}{h_1}\, c_S = -\frac{\alpha}{2\pi}\frac{L}{h_1}\log\Big[\cos\Big(\frac{\pi}{2}\Big(1-\frac{a}{L}\Big)\Big)\Big], \tag{29}$$

where $\alpha = 1$ for longitudinal flow, and 1/2 for transverse flow. In a typical application, the distance between the membrane pores, L, is smaller than the macroscopic length scale h_1. For a low-solidity membrane, $a/L \to 0$, a Taylor series expansion yields $Lc_S/h_1 \sim -(L/h_1)\log(a/L)$, which takes values on the order of unity when $h_1/L < -\log(a/L)$. This observation suggests that the hydrodynamic effect of membrane porosity will be important only in small-scale flows, such as those occurring in microscopic channels.

Acknowledgments

This research was supported by a grant provided by the National Science Foundation.

References

Larson, R.E., Higdon, J.J.L., 1986. Microscopic flow near the surface of two-dimensional porous media. 1. Axial flow. Journal of Fluid Mechanics 166, 449–472.

Larson, R.E., Higdon, J.J.L., 1987. Microscopic flow near the surface of two-dimensional porous media. 2. Transverse flow. Journal of Fluid Mechanics 178, 119–136.

Pozrikidis, C., 1997. Introduction to Theoretical and Computational Fluid Dynamics. Oxford University Press, Oxford.

Pozrikidis, C., 2001a. Shear flow over a particulate or fibrous plate. Journal of Engineering Mathematics 39, 3–24.

Pozrikidis, C., 2001b. Fluid Dynamics: Theory, Computation, and Numerical Simulation; Accompanied by the Software Library FDLIB. Kluwer Academic, Dordrecht.

Pozrikidis, C., 2002. A Practical Guide to Boundary Element Methods with the Software Library BEMLIB. Chapman & Hall/CRC, London.

Pozrikidis, C., 2004. Boundary conditions for shear flow past a permeable interface modeled as an array of cylinders. Computers and Fluids 33, 1–17.

Tachie, M.F., James, D.F., Currie, I.G., 2004. Slow flow through a brush. Physics of Fluids 16, 445–451.

Tio, K.-K., Sadhal, S.S., 1994. Boundary conditions for Stokes flows near a porous membrane. Applied Scientific Research 52, 1–20.

Wang, C.Y., 2001. Stokes flow due to the sliding of a smooth plate over a slotted plate. European Journal of Mechanics B/Fluids 20, 651–656.

Wang, C.Y., 2002. Stokes slip flow through a grid of circular cylinders. Physics of Fluids 14, 3358–3360.